Journal of Power Sources 226 (2013) 75–81

Contents lists available at SciVerse ScienceDirect

Journal of Power Sources

journal homepage: www.elsevier.com/locate/jpowsour

Short communication

Lithium storage in carbon-coated SnO_2 by conversion reaction

X.W. Guo [a,c], X.P. Fang [a], Y. Sun [a], L.Y. Shen [a], Z.X. Wang [a,*], L.Q. Chen [a,b,**]

[a] Key Laboratory for Renewable Energy, Chinese Academy of Sciences Beijing, Key Laboratory for New Energy Materials and Devices, Beijing National Laboratory for Condense Matter Physics Institute of Physics, Chinese Academy of Sciences, P. O. Box 603, Beijing 100190, China
[b] School of Materials Science and Engineering, Chonnam National University, Gwangju 500-757, Republic of Korea
[c] WPI Advanced Institute for Materials Research, Tohoku University, Sendai 980-8577, Japan

HIGHLIGHTS

- The SnO_2 and carbon-coated SnO_2 (SnO_2/C) hollow microspheres are fabricated by hydrothermal reactions respectively.
- The SnO_2/C shows higher reversible capacity and good cycling performance than that of pure SnO_2.
- A further electrochemical conversion reaction of SnO_2/C is proposed according to the experimental and theoretical evidences.

GRAPHICAL ABSTRACT

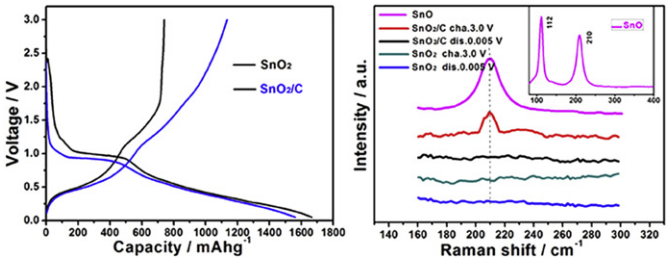

ARTICLE INFO

Article history:
Received 3 January 2012
Received in revised form
3 October 2012
Accepted 12 October 2012
Available online 3 November 2012

Keywords:
Hollow microspheres
Carbon coated tin oxide
Lithium ion battery
Raman characterization
Electrochemical conversion reaction

ABSTRACT

SnO_2 attracts considerable interest as a promising high-capacity anode material for lithium ion batteries. It is believed that SnO_2 stores lithium by the alloying and de-alloying reactions after the initial irreversible reduction from SnO_2 to Li_2O and metallic Sn. Here we report that a reversible conversion reaction, similar to that often observed in transition metal oxides, can occur in the cycling of the carbon-coated SnO_2 hollow microspheres (SnO_2/C), as is evidenced by Raman spectroscopy, high-resolution transmission electron microscopy (HRTEM) and theoretical calculations. However, only alloying and de-alloying reactions can reversibly take place in carbon-free SnO_2 hollow microspheres. The reversible capacity of the SnO_2/C is even higher than the theoretical capacity of the free SnO_2. These findings provide guidance to designing anode materials with higher reversible capacities.

1. Introduction

Lithium ion battery (LIB) is one of the most important energy storage devices for power sources of portable electronic devices and electric vehicles (EVs) [1–5]. Among the anode materials for LIBs, tin oxides (SnO_x, $x = 1$ and 2) have attracted more attention of the scientists due to their high capacity, low cost, low toxicity and high abundance [6–12].

Idoda et al. [6] first suggested SnO_2 as anode materials for LIBs in 1997. They believed that lithium can be reversibly stored in SnO_2 ($SnO_2 + xLi^+ + xe^- \leftrightarrow Li_xSnO_2$). Later we experimentally showed that SnO_2 is irreversibly reduced to Li_2O and metallic Sn in the initial discharge [13]. This explained the low initial coulombic efficiency of the material, which is one of the major obstacles to its commercial application.

$$SnO_2 + xLi^+ + xe^- \rightarrow Li_2O + Sn \quad (1)$$

* Corresponding author.
** Corresponding author. Key Laboratory for Renewable Energy, Chinese Academy of Sciences Beijing, Key Laboratory for New Energy Materials and Devices, Beijing National Laboratory for Condense Matter Physics Institute of Physics, Chinese Academy of Sciences, P. O. Box 603, Beijing 100190, China.
E-mail addresses: zxwang@iphy.ac.cn (Z.X. Wang), lqchen@iphy.ac.cn (L.Q. Chen).

0378-7753/$ – see front matter © 2012 Elsevier B.V. All rights reserved.
http://dx.doi.org/10.1016/j.jpowsour.2012.10.068

Courtney and Dahn [14] further proved that the lithium storage in SnO_x is by Li–Sn alloying and de-alloying. They proposed that the theoretical lithium storage capacity of Sn by the Li–Sn alloying is 991 mAh g^{-1}, more than twice the theoretical capacity of commercial graphite carbon.

$$Sn + xLi^+ + xe^- \leftrightarrow Li_xSn\ (0 \le x \le 4.4) \quad (2)$$

Both of the above reactions have been well accepted and become the basis for evaluating the electrochemical performances of SnO_2 anodes.

Pristine SnO_2 is a typical semiconductor with low electronic conductivity (band gap 3.6 eV). In order to improve the electronic conductivity of SnO_2, carbon is often used as a conducting phase to form a composite [8,11,15,16]. Here we report that the reversible capacity of carbon-coated SnO_2 (SnO_2/C) hollow microspheres fabricated by hydrothermal reaction following heat treatment can be well over the theoretical capacity of carbon-free SnO_2 (SnO_2). Based on careful physical analysis by Raman spectroscopy and transmission electron microscopy (TEM) and theoretical calculations, it is confirmed that a reversible conversion reaction, similar to that often observed in transition metal (TM) oxides, can occur, at least, in the first few cycles of SnO_2/C though the carbon-free SnO_2 hollow microspheres still obey the above Eq. (1) reaction.

2. Experimental section

Carbon-free and carbon-coated SnO_2 hollow microspheres were synthesized by simple hydrothermal reaction as was previously reported [4]. In a typical synthesis, $SnCl_2{\cdot}2H_2O$ dissolved in deionized water was used as the precursor. D-glucose was added to the solution and acted as a soft template in the subsequent hydrothermal reaction for 24 h at 180 °C in a Teflon-lined autoclave. Micro-scaled hollow spheres were obtained after rinsing the hydrothermal reaction product with deionized water and absolute ethyl alcohol, vacuum filtration and annealing for 2 h at 600 °C in air. For the preparation of SnO_2/C, the above SnO_2 hollow microspheres (without rinsed) were well dispersed in an aqueous glucose solution. The suspension was transferred to a Teflon-lined autoclave and heated for 3 h at 180 °C. The product was collected by centrifugation and rinsed with de-ionized water and absolute ethyl alcohol in sequence several times before dried at 80 °C for overnight. Then the resulting brown powder was carbonized at 600 °C for 10 h under inert atmosphere to obtain SnO_2/C composite hollow spheres.

The assembly of the test cells (SnO_2/$LiPF_6$-EC-DMC/Li^0) was similar to that of our previous report [4]. The mass of the active material on an 8 × 8 mm^2 copper current collector was *ca.* 2.5 mg. The cell was galvanostatically cycled between 0.005 V and 3.0 V *vs.* Li^+/Li unless otherwise specified.

The Raman spectra were recorded on a JY-T64000 instrument (Jobin Yvon Optics, France) with 532 nm laser. The FTIR spectrum of the SnO_2 discharged or recharged to various potentials was collected on FTS-60V (Bio-Rad Optics, America). The other instruments for the X-ray diffraction (XRD), field emission scanning electron microscopy (FE-SEM), transmission electron microscopy (TEM) and their configurations were the same as in our previous work [4]. The electrode materials were scraped off the Cu current collector of the cycled cells and rinsed with dimethyl carbonate (DMC) carefully before physical characterization.

To ensure the complete electrochemical oxidation or reduction of the electrode material for Raman and FTIR analysis, the test cells were firstly galvanostatically charged to the required potentials and then potentiostatically charged until the current decays to 5 μA or lower. For the discharge treatment, the cell was repeatedly galvanostatically discharged to the required potential, kept there for 10 h and then continued the discharge to the preset potential until the discharge time decays to less than 10 s. To protect the electrochemically treated samples from oxidization in air, the charged or discharged samples were sandwiched between two pieces of optical glass and sealed with Mylor-films for the Raman tests and were kept in the vacuum chamber for the FTIR test. As for the HRTEM, the scraped powder was ultrasonically dispersed in DMC and transferred to a copper grid in the Ar-filled glove box before tested. *Ab initio* density functional theory (DFT) calculations were carried out using the Vienna *ab initio* simulation package (VASP) and the values for the Gibbs formation energy were collected from the Lange's Handbook of Chemistry.

3. Results and discussion

Fig. 1 shows the XRD patterns of the carbon-free (SnO_2) and carbon-coated SnO_2 (SnO_2/C) hollow microspheres. All the diffraction peaks can be indexed to crystalline SnO_2 (JCPDS No. 88-0287). The size of the SnO_2 primary particles in the hollow microspheres is estimated to be *ca.* 20 nm according to the Scherrer equation. No reduction products were detected after carbon coating. The carbon content in the SnO_2/C hollow microsphere is determined to be 8.6 wt. % by thermogravimetric analysis (TGA) in air, much lower than what other authors have reported (27–54 wt. %) [8,11,17].

Carbon coating does not affect the other features of SnO_2. Brunauer–Emmeet–Teller (BET) measurements show no difference in either the surface area or the average pore size of these two materials (Fig. 2). The features of the as-prepared SnO_2 and SnO_2/C hollow microspheres are examined by FE-SEM and TEM. SEM imaging shows that the spherical SnO_2 (Fig. 3a) and SnO_2/C (Fig. 3b) have similar morphologies. The size of the primary SnO_2 particles is 10–20 nm, consistent with the XRD results. The wall of the sphere is *ca.* 100 nm thick (Fig. 3c and d). The crystal lattice of the SnO_2 crystallites can also be observed by HRTEM imaging (Fig. 3e). A thin and uniform carbon layer (*ca.* 2 nm in thickness) is observed on the outer surface of the SnO_2 nano-particles (Fig. 3f).

Fig. 4 compares the voltage profiles of the SnO_2 and SnO_2/C hollow microspheres in the first three cycles at a current density of 100 mA g^{-1}. The voltage profiles of the SnO_2 agree well with that of the previously reported SnO_2-based materials [7,12]. The SnO_2 and SnO_2/C electrodes show similar voltage profiles and deliver similar reversible capacities (700 mAh g^{-1}) between 0.005 and 1.5 V (insets). The voltage increases sharply if the SnO_2/Li^0 cell is further charged to over 1.7 V. The initial recharge capacity of the SnO_2

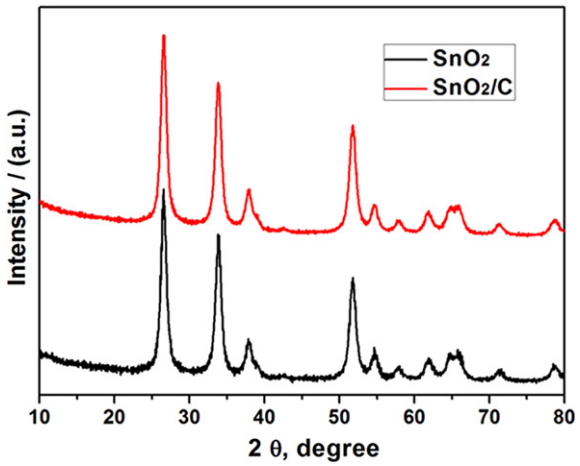

Fig. 1. Comparison of the XRD patterns of SnO_2 and SnO_2/C hollow microspheres.

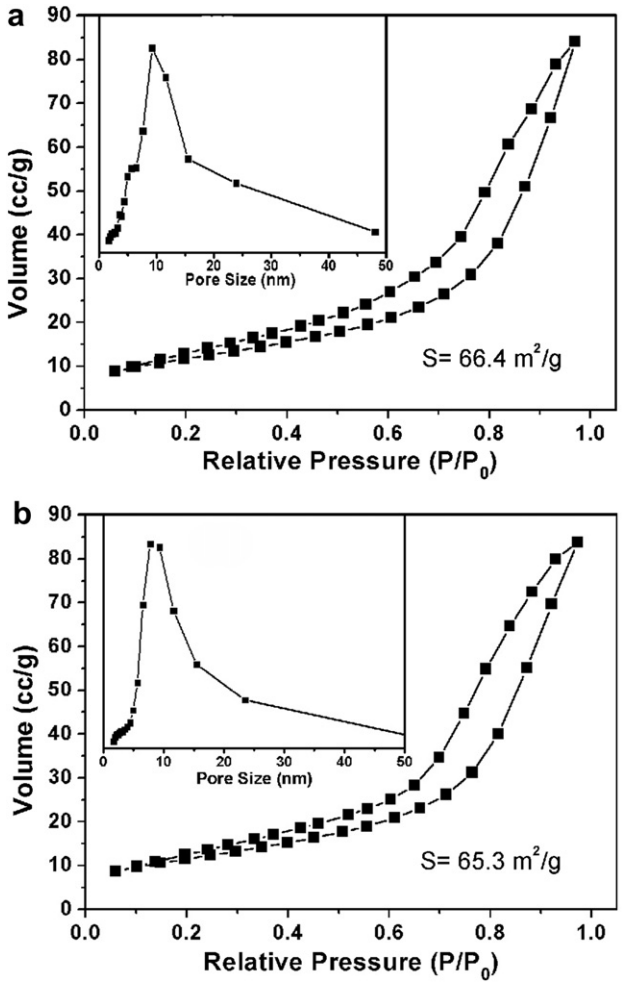

Fig. 2. The pore size distributions and surface areas of the SnO_2 (a) and SnO_2/C (b).

slightly increases to 740 mAh g^{-1} if the cell is charged to 3.0 V, corresponding to an initial coulombic efficiency of 55.4% (Fig. 4a). The large capacity loss for the initial cycle is attributed to the formation of the SEI layer and the irreversible reduction of SnO_2 to Li_2O and metallic Sn (Eq. (1)). Aggregation of the Sn nanoparticles is believed to be responsible for the capacity fading. Under similar conditions, however, the SnO_2/C electrode delivers a reversible capacity up to 1134 mAh g^{-1} in the initial cycle, 394 mAh g^{-1} more than that of the carbon-free SnO_2 (Fig. 4b). Meanwhile, the steepness of the voltage profile of the SnO_2/C electrode has no obvious change around 1.7 V, drastically different from that of the carbon-free SnO_2. These results suggest that carbon coating increases the conductivity of the SnO_2/C composite, and therefore, enhances the reversible capacity of the material. In fact, similar features in voltage profiles and reversible capacities have been observed in previous reports on carbon-coated SnO_2 electrodes [18,19]. However, it seems that no structural analysis to the recharge products or to the changes of the component of the SEI layer has ever been carried out to explore the reason for the extra capacity.

We previously reported that the SEI layer on the surface of hard-carbon/nano-Sn composite decomposed when the cell is recharged to 2.8 V or over [20]. Therefore, here we tested if decomposition of the SEI layer on SnO_2 and SnO_2/C surfaces is possible and responsible for the excess capacity of the SnO_2/C electrode above 1.5 V. Fig. 5 compares the FTIR spectra of the SnO_2 and the SnO_2/C electrodes at discharge and recharge states, respectively. Clearly an SEI layer composed of Li_2CO_3 (at 868 and 1432 cm^{-1}) and $ROCO_2Li$ (at 790, 1290 and 1636 cm^{-1}) [21,22] is formed as the cell is initially discharged to 0.005 V for both samples. However, no spectral differences are observed for these SEI species at the charge and discharge states. These indicate that the SEI layers on both the SnO_2 and the SnO_2/C are stable up to 3.0 V. Therefore, the excess capacity of the SnO_2/C material cannot be attributed to the decomposition of the SEI layer.

To our knowledge, no authors have ever reported the microstructure of the carbon-coated SnO_2 at the charged state (3.0 V). Gao et al presumed the possibility of Sn oxidation on explaining the origin for the high reversible capacity of Zn_2SnO_4 anode but did not present direct structural evidence [23]. Fig. 6 compares the Raman spectra of commercial SnO, and our pure SnO_2 and SnO_2/C at different discharge and charge states between 160 and 300 cm^{-1}. A broad peak appears at about 210 cm^{-1} (the A_{1g} mode of SnO [24,25]) in the recharged SnO_2/C electrode, evident of the presence of SnO in it. However, no such a peak is observed in the SnO_2 electrode potentiostatically charged to the same voltage. These mean that the metallic Sn is oxidized to SnO when the discharged SnO_2/C electrode is recharged to 3.0 V. This is quite similar to the conversion reaction initially reported by Tarascon and co-authors [2] and later frequently observed in many TM oxides. Besides the Raman spectroscopy, XRD was also used to recognize species in the electrode materials after discharge/charge processes. Unfortunately no obvious diffraction peaks of SnO or Sn was detected except for that of the conductive carbon black. This is clearly due to the damaged crystallinity of the cycled sample because XRD is only sensitive to crystallized phases. This often happens in transition metal oxides even after the initial discharge/recharge. In contrast, the Raman signal is sensitive to both amorphous and crystallized materials.

The oxidation of metallic Sn to SnO during recharge is confirmed by HRTEM imaging and selected area electron diffraction (SAED, Fig. 7). Domains with well-defined crystalline lattice stripes are observed in the images of both the SnO_2 and SnO_2/C electrodes. Metallic Sn, Li–Sn alloys and Li_2O (5–10 nm in size) are observed in both the discharged SnO_2 and SnO_2/C electrodes (Fig. 7a and b). Only some of the tin particles form Li–Sn alloys. This might be due to polarization of the cell, insufficiently low discharge voltage (0.005 V), and the loss of electrical contact between the current collector and some Sn nanoparticles. In the recharged carbon-free SnO_2 electrode, only Sn and Li_2O grains are observed (Fig. 7b), agreeing with our previous report [13]. On the contrary, no Li_2O is detected when the SnO_2/C electrode is recharged to 3.0 V (Fig. 7d). Rather, SnO clusters are found randomly distributed in the recharged sample, consistent with the diffused diffraction rings and the bright spots in the SAED pattern. Therefore, the HRTEM imaging and SAED suggest that SnO is one of the final products in the SnO_2/C electrodes recharged to 3.0 V. Of course, there are still some Sn domains in the recharged SnO_2/C sample. The partial oxidation of Sn is attributed to the insufficiently high conductivity of the SnO_2/C material, loss of electric contact between the Sn and Li_2O nanoparticles due to significant volume variation of the electrode, *etc.*

The above experimental results were supported with theoretical calculations. *Ab initio* density functional theory (DFT) calculations improved by DFT + U method with a self-consistent evaluation of the U parameter shows that the oxidation potential of Sn to SnO is 1.546 V, which is in good agreement with the observed values (*ca.* 1.7 V). Another simple calculation using change of Gibbs formation energy also indicates that the potential of the conversion reaction of Sn to SnO is 1.602 V [26]. These indicate that the conversion reaction is thermodynamically feasible and metallic Sn can be oxidized to SnO by the decomposition of nanosized Li_2O. With the above experimental and theoretical evidence for the possibility of Sn oxidation, we can understand why the SEI on the SnO_2 and

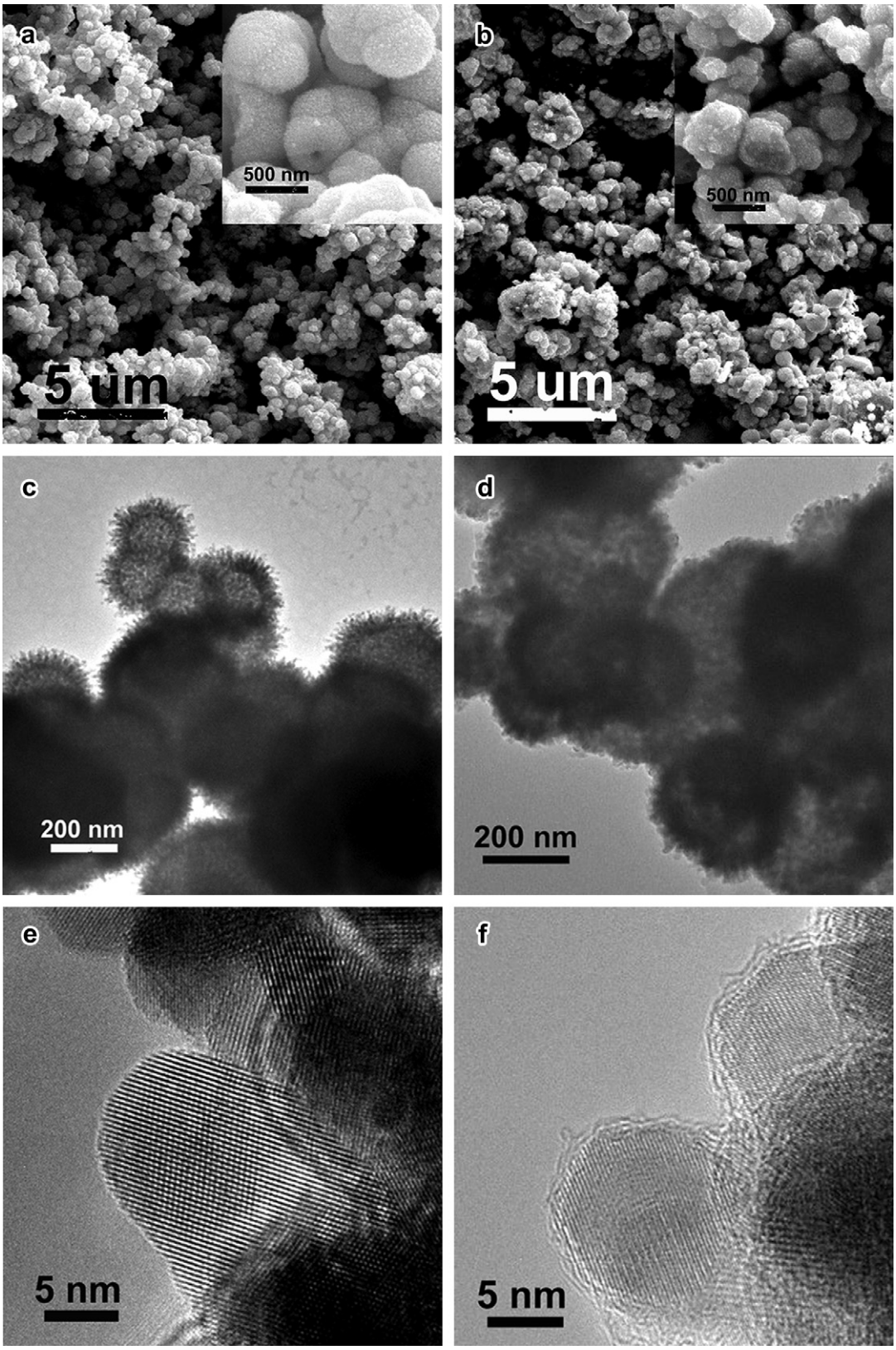

Fig. 3. The SEM, TEM and HRTEM images of the SnO_2 (a, c and e) and SnO_2/C (b, d and f).

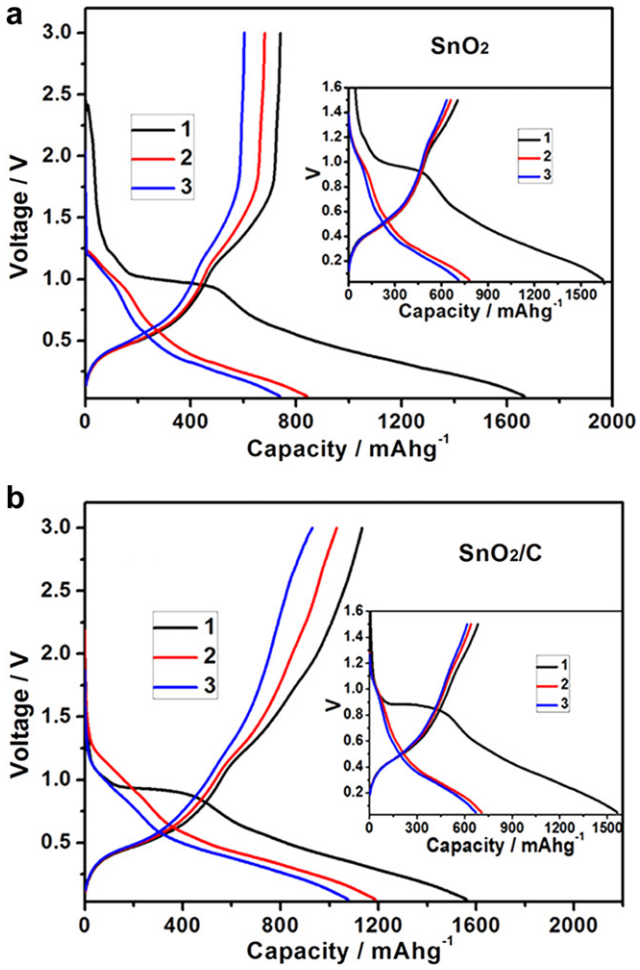

Fig. 4. The first three charge/discharge profiles of the SnO_2 (a) and SnO_2/C (b) hollow microspheres at a current density of 100 mA g^{-1} between 0.005 and 3.0 V *vs.* Li^+/Li. The insets are for their voltage profiles between 0.005 and 1.5 V *vs.* Li^+/Li.

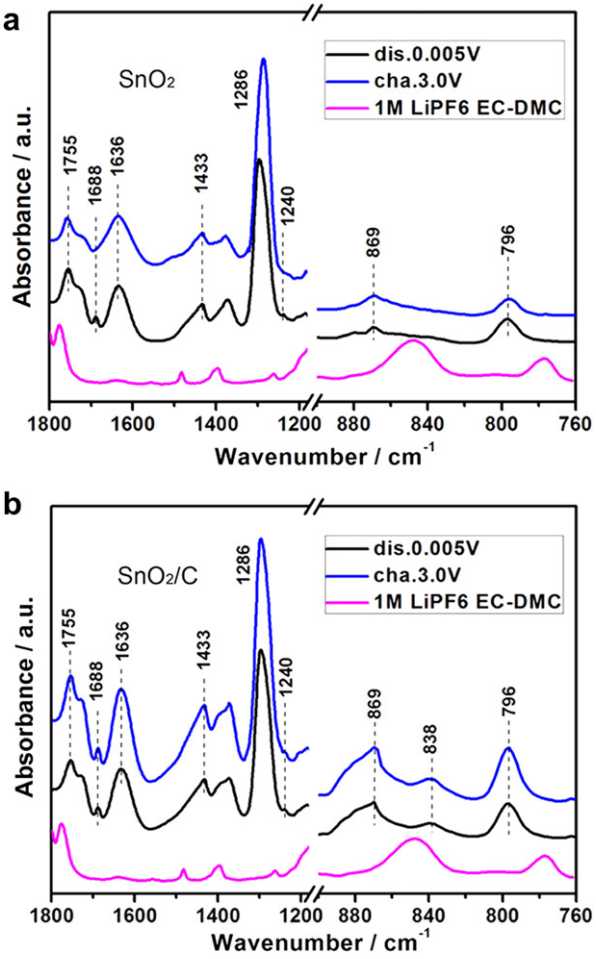

Fig. 5. Comparison of the FTIR spectra of (a) the SnO_2 and (b) the SnO_2/C discharged to 0.005 V and recharged to 3.0 V. The FTIR spectrum of the electrolyte for the cell, 1 mol L^{-1} $LiPF_6$ in EC + DMC (1:1 v/v), is shown at the bottom for reference.

SnO_2/C electrode does not decompose until 3.0 V: the Sn nano-particles/domains is oxidized to SnO (above 1.7 V *vs.* Li^+/Li) before it can catalyze the decomposition of the SEI layer (at *ca.* 2.8 V) [20].

The detection of the SnO nano-crystallites by the Raman spectroscopy, HRTEM in the recharged SnO_2/C electrode and the theoretical calculations indicate that an electrochemical conversion reaction occurs between Li_2O and metallic Sn, $Li_2O + Sn \leftrightarrow SnO + Li$. This reaction mechanism is different from the traditional understanding to the lithium storage in tin oxide electrode materials. Therefore, the following conversion reaction mechanism is proposed for the SnO_2/C system (the conversion reaction is incomplete in the present case because metallic Sn can also be found in the recharged electrode and in 0.005 V-discharged electrode).

$$Li_2O + Sn \leftrightarrow SnO + 2Li^+ + 2e^- \quad (3)$$

The theoretical lithium storage capacity corresponding to the above Eq. (3) is 398 mAh g^{-1}. Considering an extra specific capacity of 143 mAh g^{-1} is added during the first charge process of SnO_2/C, the Sn (charge product in the Eq. (2)) with the mass content of *ca.* 36% takes part in the reversible oxidation of Sn to SnO. Fig. 4 shows that the charge voltage profiles of SnO_2/C in the 2nd and 3rd cycles are more similar to that of the 1st cycle of SnO_2/C rather than that of SnO_2. Therefore, although structural analysis was only carried out

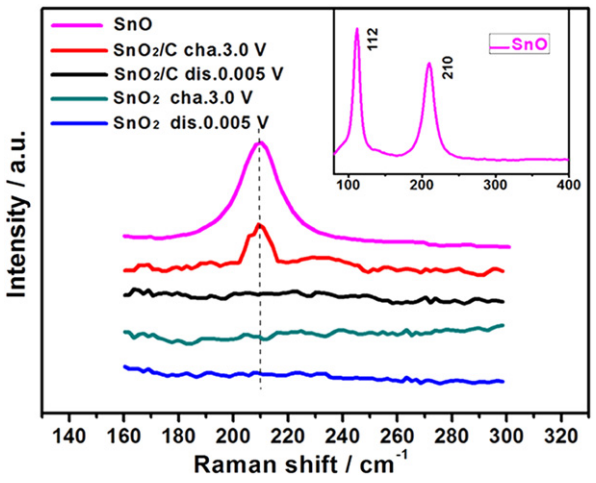

Fig. 6. Comparison of the Raman spectra of the SnO_2 and SnO_2/C electrodes discharged to 0.0 V and recharged to 3.0 V. The inset is for the Raman spectrum of commercial SnO powder for reference. The spectrum of the glass window has been subtracted from the spectra. Due to the strong Rayleigh scattering at low frequencies, observation of the vibrational peaks of metallic Sn and the low-frequency band of SnO is not possible for the poorly crystallized samples.

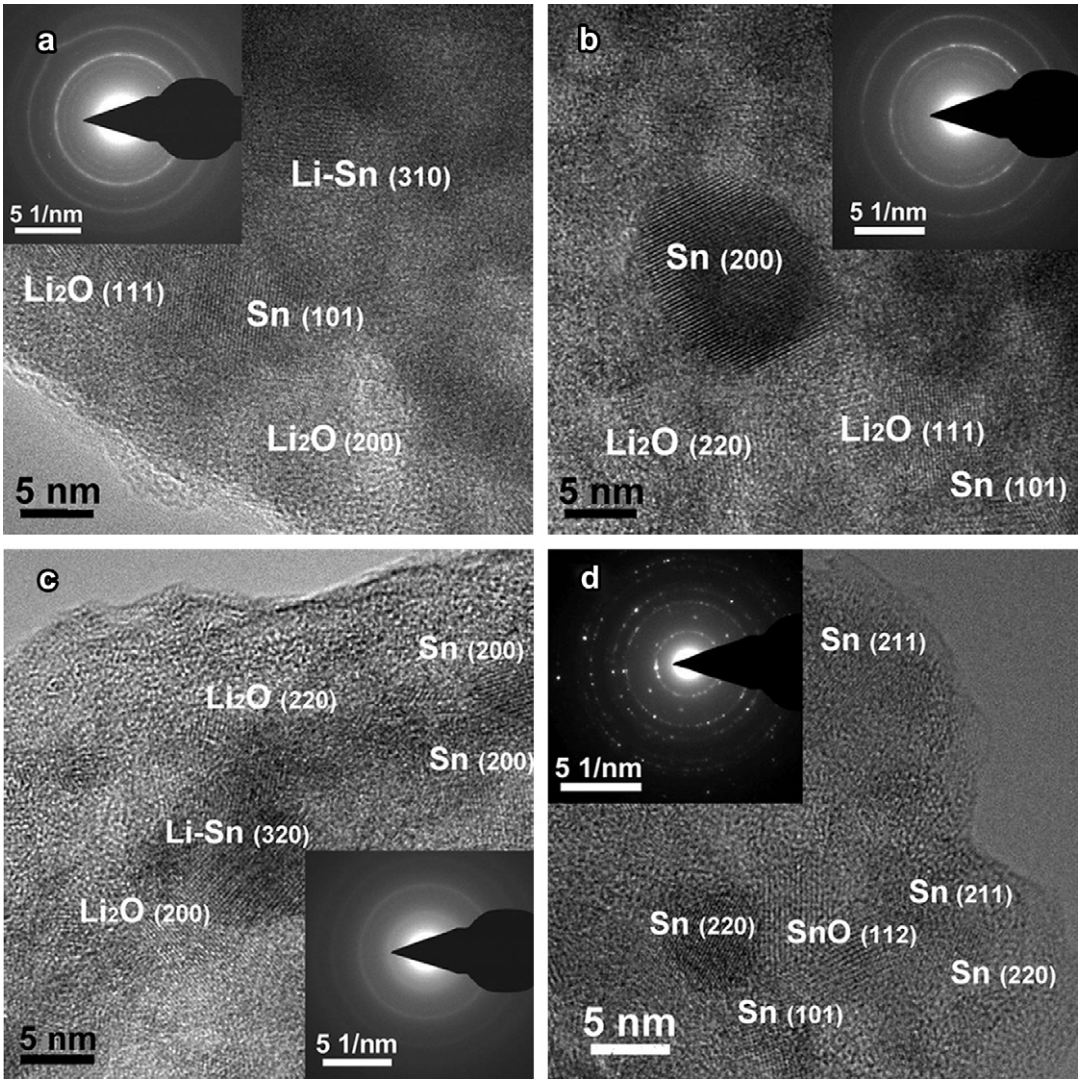

Fig. 7. The HRTEM images and SAED patterns (insets) of the products of SnO_2 (a) and SnO_2/C (b) discharged to 0.005 V, and then recharged to 3.0 V (*c* for pure SnO_2 and *d* for SnO_2/C).

on the initially discharged or recharged materials, conversion reaction is believed to occur in the subsequent cycles as well. However, this reaction decays quickly, probably due to aggregation of the nanoparticles. So it is difficult to determine experimentally how much of the Sn is oxidized and how much is not after the 1st cycle because it is not possible to calculate the capacity of the Eq. (3) and identify starting point of the above Eq. (3) in the voltage profile (Fig. 4). Fig. 8 shows that the charge capacity of the SnO_2/C material remains at 950 mAh g^{-1} in the 2nd charge and keeps higher than that of pure SnO_2 for more than 20 cycles.

The above suggestion does not agree with the previous reports on the recharge products of SnO_2 [7,8,11,12,17], where Sn were believed stable. Most of the previous researchers obtained the reversible capacity of SnO_2 with or without carbon in the voltage range between 0.005 and 1.5 V. This means that incomplete reduction/oxidation and loss of electric contact between them. So the carbon coating on the SnO_2 nanoparticles improves several properties of the composite, not only the electronic and ionic conductivity, but also the dynamics of the SnO_2 nanoparticles coated by it, and decreases the polarization of the charge/discharge processes, which is beneficial to the conversion.

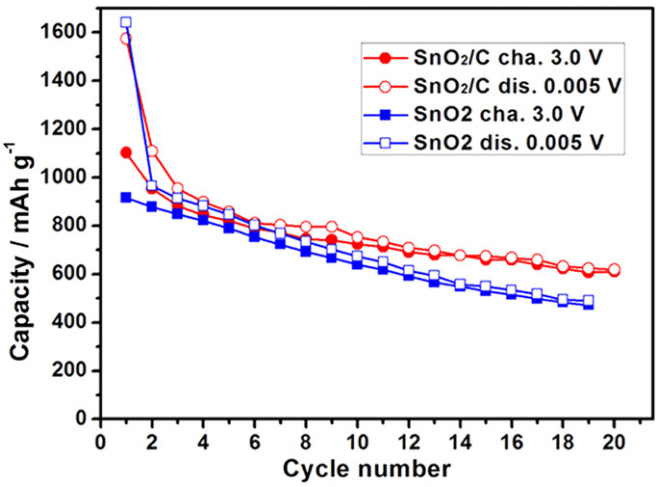

Fig. 8. Comparison of the cycling performances of pure SnO_2 and SnO_2/C electrodes between 0.005 and 3.0 V.

The above facts indicate that an electrochemical conversion reaction can also take place in non-TM oxide SnO_2/C. These findings imply that the lithium storage mechanism of a material can be modified by decreasing its polarization. With these, carbon-coated tin oxides can be a more promising anode material than the TM oxide materials because the specific capacity of the SnO_x/C is similar to that of the TM oxides but their lithium insertion potentials are lower that of the TM oxides.

4. Conclusions

Carbon-free and carbon-coated SnO_2 hollow microspheres have been fabricated by hydrothermal reaction. Although the carbon-free SnO_2 still follows the traditionally established lithium storage mechanism, the carbon-coated SnO_2 obeys a completely new lithium storage mechanism. The electrochemical oxidation of metallic tin to SnO in carbon-coated SnO_2 increases its initial coulombic efficiency and specific capacity. These findings provide guidance to the designing of tin oxide and other anode materials with improved performances.

Acknowledgments

This work was financially supported by the National 973 Program of China (2009CB220100) and the WCU (World Class University) program through the Korea Science and Engineering Foundation funded by the Ministry of Education, Science and Technology of Korea (R32-2009-000-20074-0).

References

[1] J.M. Tarascon, M. Armand, Nature 414 (2001) 359–367.
[2] P. Poizot, S. Laruelle, S. Grugeon, L. Dupont, J.-M. Tarascon, Nature 407 (2000) 496–499.
[3] P.G. Bruce, B. Scrosati, J.-M. Tarascon, Angew. Chem. Int. Ed. 47 (2008) 2930–2946.
[4] X.W. Guo, X. Lu, X.P. Fang, Y. Mao, Z.X. Wang, L.Q. Chen, X.X. Xu, H. Yang, Y.N. Liu, Electrochem. Commun. 12 (2010) 847–850.
[5] X.W. Guo, X.P. Fang, Y. Mao, Z.X. Wang, F. Wu, L.Q. Chen, J. Phys. Chem. C 115 (2011) 3803–3808.
[6] Y. Idota, T. Kubota, A. Matsufuji, Y. Maekawa, T. Miyasaka, Science 276 (1997) 1395–1397.
[7] M.S. Park, G.X. Wang, Y.M. Kang, D. Wexler, S.X. Dou, H.K. Liu, Angew. Chem. Int. Ed. 46 (2007) 750–753.
[8] X.W. Lou, D. Deng, J.Y. Lee, L.A. Archer, Chem. Mater. 20 (2008) 6562–6566.
[9] H. Li, X.J. Huang, L.Q. Chen, Electrochem. Solid-State Lett. 1 (1998) 241–243.
[10] L.H. Shi, H. Li, Z.X. Wang, X.J. Huang, L.Q. Chen, J. Mater. Chem. 11 (2001) 1502–1505.
[11] Y. Wang, F.B. Su, J.Y. Lee, X.S. Zhao, Chem. Mater. 18 (2006) 1347–1353.
[12] R. Demir-Cakan, Y.S. Hu, M. Antonietti, J. Maier, M.M. Titirici, Chem. Mater. 20 (2008) 1227.
[13] W.F. Liu, X.J. Huang, Z.X. Wang, H. Li, L.Q. Chen, J. Electrochem. Soc. 145 (1998) 59–62.
[14] I.A. Courtney, J.R. Dahn, J. Electrochem. Soc. 144 (1997) 2045–2052.
[15] J. Read, D. Foster, J. Wolfenstine, W. Behl, J. Power Sources 96 (2001) 277.
[16] L. Yuan, K. Konstantinov, G.X. Wang, H.K. Liu, S.X. Dou, J. Power Sources 146 (2005) 180.
[17] X.W. Lou, C.M. Li, L.A. Archer, Adv. Mater. 21 (2009) 2536–2539.
[18] L.Y. Jiang, X.L. Wu, Y.G. Guo, L.J. Wan, J. Phys. Chem. C 113 (2009) 14213–14219.
[19] Y. Wang, H.C. Zeng, J.Y. Lee, Adv. Mater. 18 (2006) 645–649.
[20] B.K. Guo, J. Shu, K. Tang, Y. Bai, Z.X. Wang, L.Q. Chen, J. Power Sources 177 (2008) 205–210.
[21] D. Aurbach, M.L. Daroux, P.W. Faguy, E. Yeager, J. Electrochem. Soc. 134 (1987) 1611–1620.
[22] D. Aurbach, Y. Ein-Eli, B. Markovsky, A. Zaban, S. Luski, Y. Cameli, H. Yamin, J. Electrochem. Soc. 142 (1995) 2882–2890.
[23] A. Rong, X.P. Gao, G.R. Li, T.Y. Yan, H.Y. Zhu, J.Q. Qu, D.Y. Song, J. Phys. Chem. B 110 (2006) 14754–14760.
[24] J. Geurts, S. Rau, W. Richter, F.J. Schmitte, Thin Solid Films 121 (1984) 217–225.
[25] L. Sangaletti, L.E. Depero, B. Allieri, F. Pioselli, E. Comini, G. Sberveglieri, M. Zocchi, J. Mater. Res. 13 (1998) 2457–2460.
[26] H. Li, P. Balaya, J. Maier, J. Electrochem. Soc. 151 (2004) A1878–A1885.